Chapter 8
Spanning Fullerenes as Units in Crystal Networks

Mircea V. Diudea and Beata Szefler

Abstract Fullerenes are molecules consisting of tri-connected polyhedral cages of various covering. Spanning fullerenes can be obtained by deleting some atoms or bonds, thus resulting in open structures with di-connected atoms which can further join to atoms of the same or different repeating units in construction of crystal- or quasicrystal-like networks. In this chapter, a variety of spanning fullerenes, designed either by opening cages or by sequences of map operations, are used to build more complex nanostructures. Energetics of some spanning fullerenes has been calculated on optimized structures at Hartree-Fock and/or DFT level of theory. The topology of crystal networks is described in terms of Omega polynomial.

8.1 Introduction

Fullerenes are molecules consisting of tri-connected polyhedral cages of various coverings or tessellations. When there is a single type of polygonal faces, the covering is called Platonic; when there are two types of faces, the covering is called Archimedean (Diudea 2010a). A molecule can be represented by a molecular graph. A *graph* $G(V, E)$ is an ordered pair of two sets, V and E, $V = V(G)$ being a finite nonempty set and $E = E(G)$ a binary relation defined on V (Harary 1969; Diudea et al. 2002). A graph can be visualized by representing the elements of V by points (i.e., vertices) and joining pairs of vertices (i, j) by a bond (i.e., edge) if and only if $(i, j) \in E(G)$. The number of vertices in G equals the cardinality $v = |V|$ of this set.

M.V. Diudea (✉)
Faculty of Chemistry and Chemical Engineering, Babes-Bolyai University, 400028 Cluj, Romania
e-mail: diudea@gmail.com

B. Szefler
Department of Physical Chemistry, Collegium Medicum, Nicolaus Copernicus University, Kurpińskiego 5, 85-950 Bydgoszcz, Poland
e-mail: beatas@cm.umk.pl

A.R. Ashrafi et al. (eds.), *Topological Modelling of Nanostructures and Extended Systems*, Carbon Materials: Chemistry and Physics 7, DOI 10.1007/978-94-007-6413-2_8,

A graph is said connected if any two vertices, i and j, are the endpoints of a path; otherwise, it is disconnected. The molecular graphs are in general connected graphs.

Spanning fullerenes can be designed by deleting, from their molecular graph, some vertices/atoms or edges/bonds, thus resulting in open structures with di-connected atoms which can further be joined with atoms of the same or different repeating units in designing *periodic nanostructures*, as those encountered in nano-dendrimers, in crystals or quasicrystals. Note that spanning of fullerenes can be obtained in laboratory by irradiating the closed cages by electron or ion beams, while many of the molecular constructions to be presented in the following can be seen as potentially real structures. Since fullerenes can be designed from the Platonic polyhedra, tetrahedron T, cube C, octahedron Oct, dodecahedron Do, and icosahedron Ico, by applying some operations on maps, the spanning fullerenes can be designed by such sequences of operations, the "opening" Op operation included.

A map is a discretized (closed) surface. Among the most important map operations we mention are the following: dual *Du*, medial *Med*, P_k-mapping, $k = 3$–5, *Leapfrog Le*, *Chamfering Q*, and *Capra Ca*. These operations are implemented in the CVNET software package (Stefu and Diudea 2005). More about map operation the reader can find in Diudea (2010a) and Stefu et al. (2005).

Dendrimers are hyper-branched structures with a well-tailored architecture. Their endgroups can be functionalized, thus modifying their initial properties. Dendrimers have gained a wide range of applications in supramolecular chemistry, particularly in host-guest reactions and self-assembly processes. Promising applications come from polyamidoamine dendrimers as gene transfer vectors and peptide dendrimers as antipeptide antibodies and synthetic vaccines (Diudea 2010a, p. 80).

The number of edges emerging from each branching point is called the *progressive degree* (Diudea and Katona 1999), p (i.e., the edges increasing the number of points of a newly added generation). It equals the classical vertex degree d minus 1: $p = d - 1$.

The stepwise growth of a dendrimer follows a mathematical progression. A first problem in studying the topology of dendrimers is that of enumerating its constitutive parts: vertices, edges, or fragments.

The number of vertices in the ith orbit (i.e., that located at distance i from the center) of a regular dendrimer can be expressed as a function vertex degree d:

$$v_i = (2 - z)(d + z - 1)(d - 1)^{(i-1)}; \quad i > 0 \tag{8.1}$$

where $z = 1$ for a monocentric dendrimer and $z = 0$ for a dicentric one. By using the progressive degree p, relation (8.1) becomes

$$v_i = (2 - z)(p + z)p^{(i-1)}; \quad i > 0 \tag{8.2}$$

For the core, the number of vertices is $v_0 = 2 - z$, while the number of external vertices (i.e., the endpoints) is obtained by

$$v_r = (2 - z)(p + z)p^{(r-1)} \tag{8.3}$$

where r is the radius of the dendrimer and equals the number of its orbits/generations.

The total number of vertices $v(D)$, in dendrimer, is obtained by summing the populations on all orbits:

$$v(D) = (2-z) + (2-z)(p+z)\sum_{i=1}^{r} p^{(i-1)} \tag{8.4}$$

By developing the sum in (8.4), one obtains

$$v(D) = (2-z) + (2-z)(p+z)\left(\frac{p^r-1}{p-1}\right) = \frac{2(p^{r+1}-1)}{p-1} - zp^r \tag{8.5}$$

A useful recurrence enables one to calculate $v(D)$ from the number of vertices of the precedent term of a dendrimer family (i.e., a homologous series of dendrimers, having the same progressive degree, p) $v(D_{r+1}) = pv(D_r) + 2$, irrespective of monocentric or dicentric the dendrimer is.

The term nano-dendrimer refers here to hyper-branched structures of which branching nodes represent nanotube junctions (i.e., spanned fullerenes), while the bonds joining them are nanotubes of various length.

Crystals are (MacKay 1981; Hargittai and Hargittai 2010) periodic structures, of which (one-type) unit cells, consisting of one or more atoms or other identical components, repeat a large number of times by three noncoplanar translations. Corresponding atoms in each unit cell have almost identical surrounding, while the fraction of atoms near the surface is small and the effects of the surface can be neglected.

Quasicrystals are quasiperiodic structures (Levine and Steinhardt 1984), showing more than one type of repeating unit, or the same unit repeating quasi-regularly. Quasicrystals can have the topology of multi-tori, particularly of those with icosahedral symmetry. These kinds of periodic structures will be exemplified in the following.

Multi-tori are structures of high genera, consisting of more than one tubular ring (Diudea and Petitjean 2008). They are supposed to result by self-assembly of some repeat units or monomers; their geometry is eventually superimposed on surfaces of negative curvature, like FRD or P-surface, and shows a high porosity. Multi-tori can be designed starting from small cages, for example, the Platonic solids. Modeling of porous structures has been previously reported by Mackay and Terrones (1991), Lenosky et al. (1992) and Terrones and Mackay (1993), etc. Such structures appear in spongy carbon (already synthesized, Benedek et al. 2003), in schwarzites (named in honor of mathematician Schwarz 1865, 1890), or in zeolites (natural aluminosilicates).

8.2 Design of Spanning Fullerenes

There are at least two ways to design a tubular nano-junction: (1) by sequences of map operations and (2) by spanning appropriate fullerenes.

8.2.1 Junctions by Map Operations

Three basic map operations Leapfrog *Le*, Chamfering (Quadrupling) *Q*, and Capra *Ca* (the reader is invited to consult: Diudea 2004, 2005; Diudea et al. 2003, 2006a; Stefu et al. 2005), associated with the opening *Op* operation, are most often used to transform small polyhedral objects (basically, the Platonic solids) into tubular junctions (Diudea and Nagy 2007). These transforms preserve the symmetry of the parent map. Figure 8.1 presents a realization by Leapfrog *Le* operation (Nagy et al. 2011).

8.2.2 Junctions by Spanning Fullerenes

Spanning a fullerene graph can be done by deleting/braking some edges (and vertices), thus getting a particular patch (eventually identical to a circulene molecule). Figure 8.2 illustrates the case of coronene-preserving opening (left) and sumanene-preserving opening (right) of fullerene $C_{84}\_20-T_d$ (Diudea 2010b). Figure 8.3 presents three octahedral nano-junctions derived from the hypothetical fullerene C_{168} that consists of eight (disjoint) sumanene patches (Szefler et al. 2012a), lying in the corners of cube, while on cube faces having octagons, Sum_CZ_192 and Sum_CA_216 are obtained by opening operations *Op*(1a) and *Op*(2a), respectively; the third one, Sum_OctS_2LeX_168, results by simply deleting the alternating edges of octagon, *Op*(−a). Observe that the last numbers in the name of structures represent the number of carbon atoms. Other particular monomeric units will be presented below.

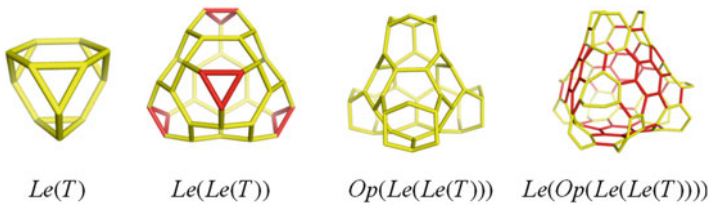

Fig. 8.1 Design of a tetrapodal junction by Leapfrog *Le* map operation

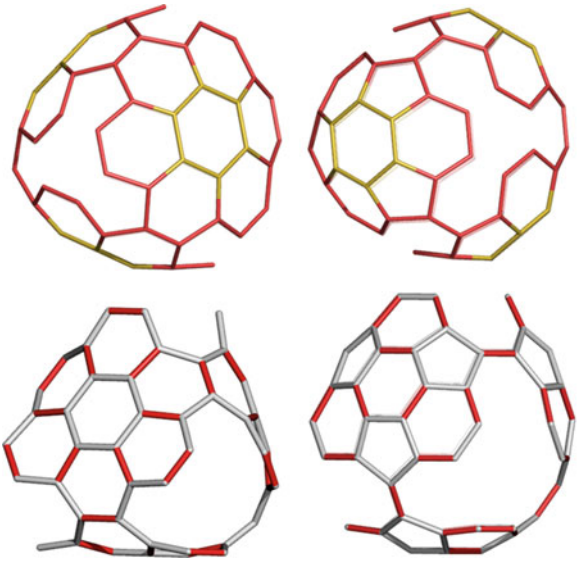

Fig. 8.2 Opening C_{84}_20-T_d: as coronene, 4[6:6_6], $v = 84$, $e = 114$, $f_6 = 28$, $g = 2$ (*left* – also designed by the sequence of map operations – see Fig. 8.1) and sumanene, 4[6:$(5,6)_3$], $v = 84$, $e = 114$, $f_5 = 12$, $f_6 = 16$, $g = 2$ (*right*) patches, respectively; optimized structures are shown in the *bottom row*

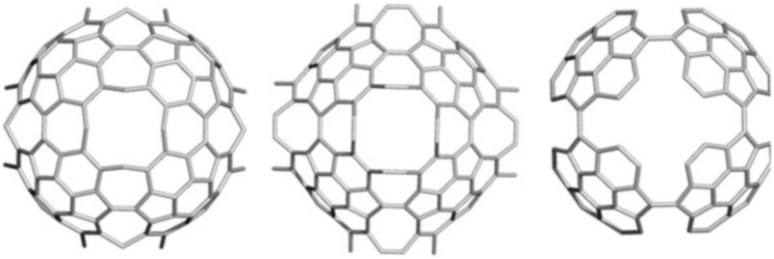

Fig. 8.3 Sumanene motif decorating octahedral nano-junctions: Sum_CZ_192 (*left*), Sum_CA_216 (*middle*), and Sum_OctS_2LeX_168 (*right*)

The spanned cages can be used to build dendrimers or other periodic nanostructures by joining with other units (the same or not) or by identifying common substructures (see below).

Table 8.1 lists the energetics of these hypothetical nano-junctions, optimized at the Hartree-Fock level of theory, as hydrogen-ended molecules. When compared to the values for C_{60}, the reference structure in nanoscience, one can see the spanned fullerenes show at least (or higher) the stability of the reference. The extent of strain, as given by POAV theory (Haddon 1987, 1990), is favorable for the opened fullerenes (Table 8.1, last column) in comparison to that of C_{60}, the structures included in this table being real candidates to the status of real molecules.

Table 8.1 Total energy E_{tot} and HOMO-LUMO gap, at Hartree-Fock HF (HF/6-31 G(d,p)) level of theory, for some hypothetical nano-junctions and C_{60} reference nanostructure

	Structure	E_{tot} (au)	E_{tot}/C (au/mol)	HF_gap (eV)	POAV/C (kcal/mol)
1	Cor_T_84	−3,194.767	−38.033	7.347	1.477
2	Sum_T_84	−3,155.466	−38.028	7.562	1.685
3	Sum_CZ_192	−7,298.367	−38.012	6.044	1.049
4	Sum_CA_216	−8,206.401	−37.993	6.442	0.550
5	Sum_OctS_2LeX_168	−6,389.018	−38.030	6.637	0.821
6	C_{60}	−2,271.830	−37.864	7.418	8.256

8.3 Dendrimers

Dendrimers (Fig. 8.4) can be designed from monomers with tetrahedral symmetry, either by joining the two-connected terminal vertices or by identification of appropriate (open) faces (Diudea 2010b). Dendrimers at 2nd generation are illustrated in Fig. 8.5 (Diudea 2010c).

The corresponding dimers (Fig. 8.6, top) are "intercalated" ones. A possible linear evolution of the above monomers is presented in Fig. 8.6, bottom (Diudea 2010b).

Other examples come from polybenzenes (Fig. 8.7), which are nanostructures consisting of benzene ring as the main motif (O'Keeffe et al. 1992) of tessellation.

8.4 Crystal-Like Networks

When monomers have octahedral symmetry, they can embed in the P-type surface in getting crystal-like networks which belong to the space group P_n3m. Figure 8.8 illustrates nets showing the sumanene 6:$(5,6)_3$ motif (Szefler et al. 2012a).

Other examples of crystal-like networks are given in Fig. 8.9 (Szefler and Diudea 2013): their covering consists of motifs of hexagon triples (unit C_3HexZ_104) and heptagon triples (unit C_3HepA_104), respectively, for which the energetic data are given in Table 8.2.

Again the open structures (i.e., nano-junctions) appear less strained than the reference C_{60} fullerene and, according to the total energy (calculated on the optimized structures at Hartree-Fock HF and DFT levels of theory) and HOMO-LUMO gap, are at least as stable as the reference molecule. The strain of heptagon triple motif is one order of magnitude lower than that of hexagon triple one and two orders of magnitude lower than that of the reference fullerene, also reflected in the values of TE/C. In view of a possible identification among nano-materials, IR and RAMAN spectra have been simulated (Szefler and Diudea 2013). Polybenzenes can also be embedded in the P-type surface (Fig. 8.10).

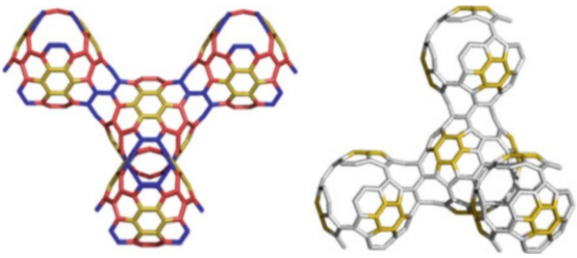

Fig. 8.4 Dendrimers by monomers with coronene (*left*) and sumanene (*right*) motifs, at 1st generation

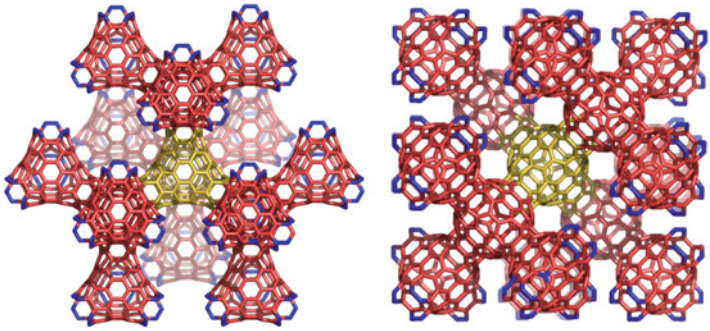

Fig. 8.5 Dendrimer with coronene motif at 2nd generation (two different views)

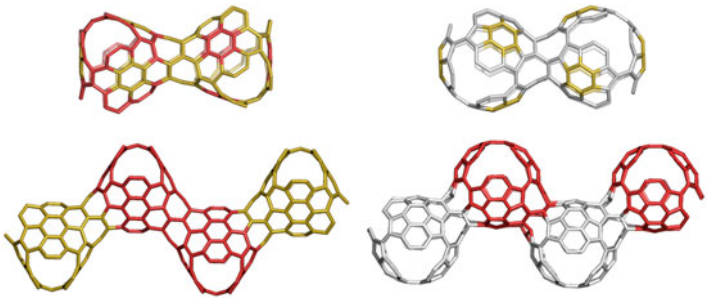

Fig. 8.6 Linear evolution of the monomers with coronene (*left column*) and sumanene (*right column*) motifs

D-type surface can also embed a polybenzene structure (Fig. 8.11). This last net shows the topology of D_6-diamond: a face-centered cube f_{cc}-structure, belonging to the space group *Pn*3*m* (Szefler and Diudea 2012).

Calculations have been performed at HF/6-31 G(d, p) and B3LYP/6-311 + G(d, p) level of theory, respectively, on Gaussian 09 software package (2009).

Stability of the monomers and the corresponding dimmers with respect to the reference C_{60} fullerene can be compared from data in Table 8.3. Note the three types of dimers originating in BTA_48, function of the identified face/ring and

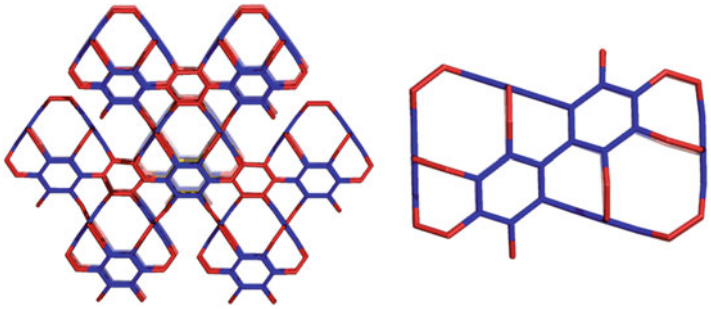

Fig. 8.7 Polybenzene dendrimer (*left*) and its "intercalated" dimer (*right*)

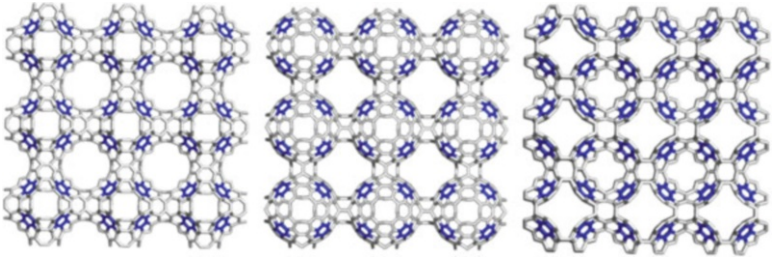

Fig. 8.8 P-type surface embedding of monomers in Fig. 8.3: Sum_CA_216 (*left*), Sum_CZ_192 (*middle*), and Sum_OctS_2LeX_168 (*right*)

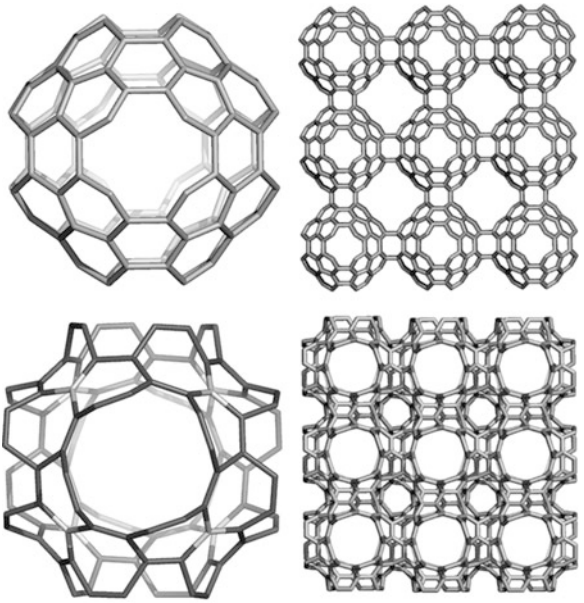

Fig. 8.9 *Top row*: C_3HexZ_104 ($v = 104$; $e = 144$; $f_6 = 36$; $g = 3$) and its p-type crystal-like net ($v(3,3,3) = 2{,}808$); *bottom row*: C_3HepA_104 ($v = 104$; $e = 132$; $f_7 = 24$; $g = 3$) and its p-type crystal-like net (junctions designed by map operation sequences $Op_{2a}(S_2(\mathrm{C}))$ and $Op(S_1(\mathrm{C}))$, respectively)

Table 8.2 Energies (total energy per carbon atom TE/C, in Hartree H; HOMO-LUMO gap, HL gap, in electron volts; POAV strain energy per carbon atom S/C, kcal/mol) of the optimized structures at HF and DFT level of theory

	Molecule	Carbon atoms	TE/C (H)	HL gap (eV)	POAV/C (kcal/mol)
HF					
1	C_3HexZ_104	104	−37.999	5.342	2.329
2	C_3HepA_104	104	−38.127	6.942	0.240
3	C_{60}	60	−37.864	7.418	8.256
DFT					
4	C_3HexZ_104	104	−38.244	1.658	2.352
5	C_3HepA_104	104	−38.376	1.354	0.192
6	C_{60}	60	−38.110	2.724	8.256

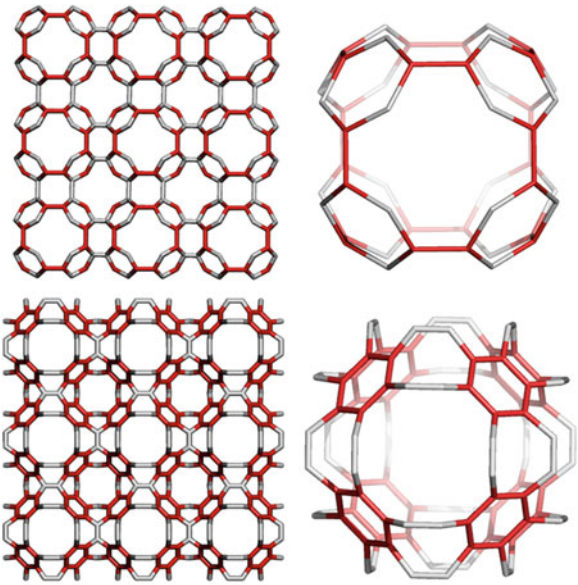

Fig. 8.10 Polybenzenes embedded in the P-type surface: *p*-BCZ_48 (*top*) and *p*-BCA_96 (*bottom*) and the corresponding units (*right column*)

conformation: (BTA_48)2_84_dendrim (R_{12}, intercalate, Table 8.3, entry 2, and Fig. 8.7, right), (BTA_48)2_88_ f_{cc} (R_8, Table 8.3, entry 3, and Fig. 8.11, right), and (BTA_48)2_90_MT (R_{12}, eclipsed, Table 8.3, entry 4, and Fig. 8.12, bottom, left) (Szefler et al. 2012b).

One can see that the strain in polybenzenes, as calculated by POAV theory, is far less than that in C_{60}, and the overall stability is at least as that of the reference fullerene. Infrared and Raman spectra have been simulated (Szefler et al. 2012b) in view of possible use in laboratory identifying such structures, tessellated with the simplest benzene ring motif. The high values of HOMA index of aromaticity (Krygowski and Ciesielski 1995, 1996), in the last column of Table 8.3, suggest that the benzene ring geometry is not too much modified in comparison to the

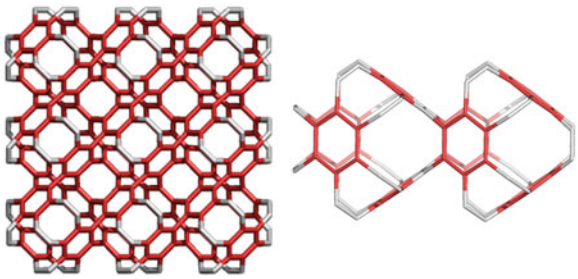

Fig. 8.11 Polybenzene embedded in the D-type surface: f_{cc}-BTA_48 and its f_{cc}-dimer (*right*)

Table 8.3 Total energy E_{tot} per atom (kcal/mol) and HOMO-LUMO gap, at Hartree-Fock HF level of theory, strain by POAV theory and HOMA index in benzene-patched units and their dimers and C_{60} reference structure, as well

	Structure	No. units	E_{tot}/(au)	E_{tot}/atom (au)	HL gap (eV)	POAV/C (kcal/mol)	HOMA (R[6])
1	BTA_48	1	−1,831.484	−38.156	11.285	0.083	0.951
2	(BTA_48)2_84_dendrim	2	−3,201.679	−38.115	10.895	0.061	0.975
3	(BTA_48)2_88_f_{cc}	2	−3,355.431	−38.130	10.970	0.074	0.972
4	(BTA_48)2_90_MT	2	−3,428.847	−38.098	10.085	0.220	0.957
5	BCZ_48	1	−1,831.097	−38.148	8.134	3.395	0.989
6	(BCZ_48)2_96	2	−3,657.417	−38.098	7.043	2.842	0.114
7	BCA_96	1	−3,662.991	−38.156	10.253	0.124	0.939
8	(BCA_96)2_184	2	−7,013.828	−38.119	9.805	0.180	0.936
9	C_{60}	1	−2,271.830	−37.864	7.418	8.256	0.493

free benzene molecule (HOMA value = 1), while the hexagonal rings in C_{60} are much more affected (HOMA = 0.493) by the presence of pentagons (see also Cysewski and Szefler 2010). The HOMA value is even dropped in case of dimer (BCZ_48)2_96 (Table 8.3, entry 6) because the units bound directly at the benzene ring. The loss in pi-electron resonance is partly compensated by the loss in strain energy, visible when compared with the BCZ_48 unit (Table 8.3, entry 5). However, in an infinite network, the strain will drop even more (Szefler et al. 2012b), and the geometry approaches to that of the unit-free molecule.

8.5 Quasicrystal Nanostructures

Multi-tori are designed by using "eclipsed" dimers (Diudea and Nagy 2007), as shown in Fig. 8.12, bottom row. The dimer BMTA2_90 was included in Table 8.3 (as (BTA_48)2_90_MT, entry 4). The unit BTZ_24, due to its simplicity, can form only the dimer BMTZ2_48, leading to multi-tori. The multi-tori bearing the benzene patch will have B as a prefix in their name. Next, because theopening faces show

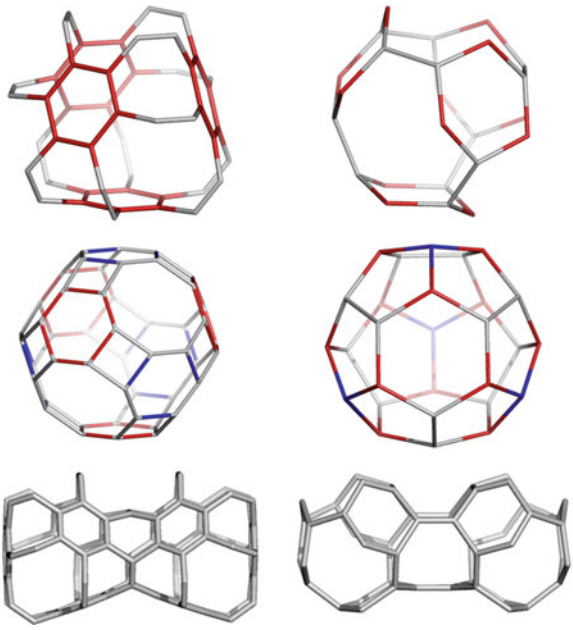

Fig. 8.12 *Left column*: BTA_48 (*top*) formed by spanning the cage Le(P_4(T))_48 (by deleting the *blue bonds* – *middle*) and its multi-torus BMTA2_90 dimer ((BTA_48)2_90_MT in Table 8.3, entry 4). *Right column*: BTZ_24 (*top*) originating in S_2(T)_28 = C_{28} (the four *blue* points located at the center of pentagon triples to be deleted – *middle*) and its multi-torus BMTZ2_48 dimer

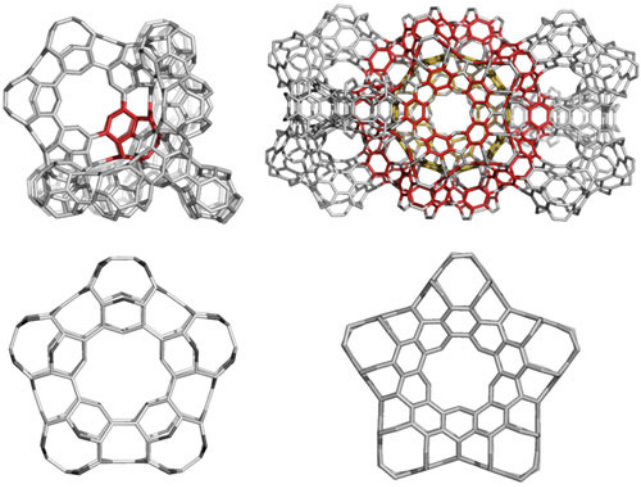

Fig. 8.13 *Left column*: BMTZ17_408 and its hyper-pentagon MMTZCy5_120. *Right column*: BMTA34_1332 and its hyper-pentagon BMTACy5_210

either "zigzag" or "armchair" endings, "Z" or "A" will be added as a suffix to their name. The number of repeating units and/or number of atoms will be added after the letters.

The BMTX2 dimers, because of their "eclipsed" conformation, will form pentagonal hyper-rings BMTXCy5 (Fig. 8.13, bottom) in a self-assembly process.

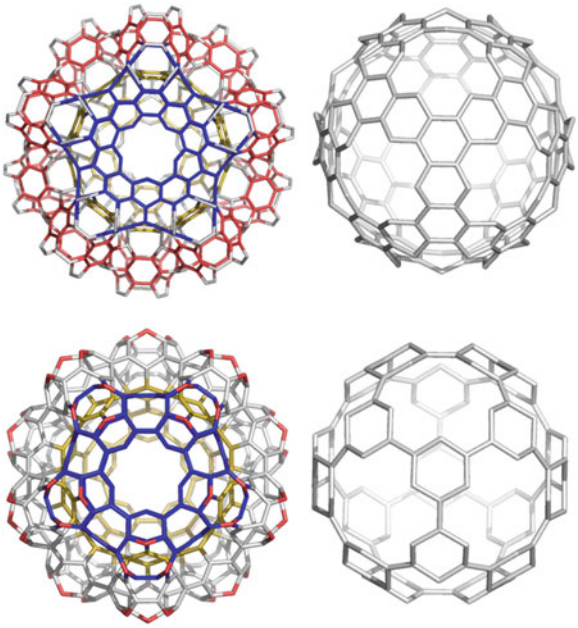

Fig. 8.14 *Top row*: multi-torus BMTA20_1_780 (*left*) and its core ($-f_5(Le_{2,2}(\mathrm{Do}))$, *right*); *bottom row*: multi-torus BMTZ20_1_480 (*left*) and its core ($-d_5(\mathrm{S}_2(\mathrm{Ico})$, *right*))

These can further evolve to the multi-torus BMTX17 (X = Z, Fig. 8.3, left), of which reduced graph is just C_{17}, the structure proposed by Diudea (2010d) as the seed for the diamond D_5. By analogy to D_5, a hyper-dimer BMTX34 can be designed (X = A, Fig. 8.3, right). We mention that its reduced graph is C_{34}, the repeating unit of the triple periodic structure of D_5. Recall that D_5 is an *mtn* triple periodic 3-nodal net, named ZSM-39 (a structure found in clathrates of type II), of point symbol net: $\{5^5.6\}12\{5^6\}5$ and $2[5^{12}] + [5^{12}.6^4]$ tiling. It is also known as the *f*cc_C_{34} structure (Blase et al. 2010; Diudea et al. 2011), because of its face-centered cubic lattice that belongs to the space group *Fd3m*. Thus, we can expect a 3D network derived from these benzene-patched units, similar to D_5.

A spherical multi-torus BMTX20 (Fig. 8.14, left column) can be constructed and is a $g = 21$ multi-torus, with a well-defined core: Core(BMTA20)_180 = $-f_5(Le_{2,2}$ (Do)) while Core (BMTZ20)_120 = $-d_5(\mathrm{S}_2(\mathrm{Ico})$. In the above, $-f_5$ means deletion of all pentagonal faces in the Leapfrog (2,2) transform of the dodecahedron Do, and $-d_5$ is deletion of vertices of degree $d = 5$, in the transform of Icosahedron = Ico by the septupling S_2 operation. Also, $-d_5(\mathrm{S}_2(\mathrm{Ico})) = Op(Le(\mathrm{Ico}))$. Recall that g is the genus of the surface that embeds a structural graph and accounts for the number of simple tori of which consists that graph (Diudea and Szefler 2012).

A linear array BMTX20_*k*, $k = 1,2,\ldots$ with the repeating unit formed by two units superimposing one pentagonal hyper-face (i.e., BMTXCy5), rotated to each other by an angle of pi/5 as in the "dimer" BMTA20_2 (Fig. 8.15, top, left). Next, the structure can evolve with a one-dimensional periodicity, as shown in BMTA20_4 (Fig. 8.15, top, right) or in the hyper-cycle BMTZCy20_5 (Fig. 8.15, bottom, left).

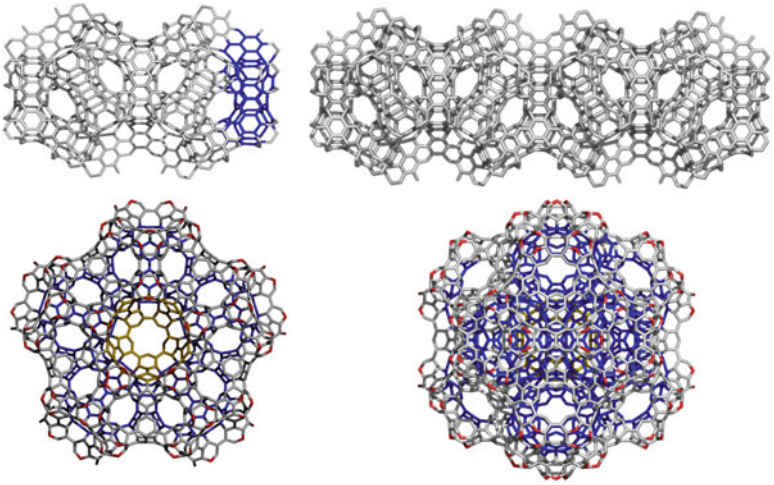

Fig. 8.15 *Top row*: the repeat unit BMTA20_2_1350 (*left*) and a rodlike BMTA20_4_2490 (*right*); *bottom row*: multi-tori BMTZCy20_5_1800 (*left*) and BMTZSp20_12_3120 (twofold symmetry)

Twelve units of BMTX20 can form a spherical array (of icosahedral symmetry), as in case of BMTZSp20_12 (Fig. 8.15, bottom, right), of which core is just BMTZ20 (a 13th unit).

Theorem 8.1 *In multi-tori built up from open tetrahedral units, the genus of structure equals the number of its units plus one, irrespective of the unit tessellation.*

Demonstration comes out from construction and is illustrated on the multi-tori BMTXCy5 (Fig. 8.13, bottom row): there are five units open to be inserted in exactly five simple tori and one more torus that join all the above five units, thus demonstrating the first part of the theorem (Diudea and Szefler 2012).

For the second part, we apply the Euler's theorem (1758):

$$v - e + f = \chi = 2(1 - g) \tag{8.6}$$

where $v = |V(G)|$ is the number of vertices/atoms, $e = |E(G)|$ is the number of edges/bonds, and f is the number of faces of the graph/molecule. In the above, g is the *genus* of the (orientable) surface S on which a molecular graph is embedded. The genus is related to the Gaussian curvature of the surface S by means of Euler's characteristic χ of S (Gauss-Bonnet 1853) theorem as for $g = 0$ (case of sphere) $\chi > 0$ (positive curvature); for $g = 1$ (case of torus) $\chi = 0$, while for $g > 1$ (surfaces of high genera), $\chi < 0$, S will show a negative curvature. More about surfaces of negative curvature the reader can find in Diudea and Nagy (2007).

To complete the demonstration, we will use the data in Table 8.4 providing the values of g in several BMTX multi-tori, tessellation differing as X = A or Z.

The number of tetrahedral units BMTX1 in the linear array of BMTX20_k (Table 8.4, entries 3–6) is $u = 20k - 5(k-1) = 15k + 5$, according to the construction mode. The term $-5(k-1)$ accounts for the superimposed hyper-

Table 8.4 Euler formula calculation in multi-tori BMTX

	BMTX	v	e	f_6	f_8	f_{tot}	$2(1-g)$	g	u	u-formula
1	BMTACy5	210	285	35	30	65	−10	6	5	$f_8/6$
2	BMTZCy5	120	165	20	15	35	−10	6	5	$f_6/4$
3	BMTA20_1	780	1,110	170	120	290	−40	21	20	$f_8/6$
4	BMTZ20_1	480	690	80	90	170	−40	21	20	$f_6/4$
5	BMTA20_5	3,060	4,410	710	480	1,190	−160	81	80	$f_8/6$
6	BMTZ20_5	1,920	2,790	320	390	710	−160	81	80	$f_6/4$
7	BMTZCy20_5	1,800	2,625	300	375	675	−150	76	75	$f_6/4$
8	BMTZ20_12	4,440	6,465	740	915	1,655	−370	186	185	$f_6/4$
9	BMTZSp20_12	3,120	4,590	520	690	1,210	−260	131	130	$f_6/4$

rings, BMTXCy5. In case of BMTZCy20_5 (Table 8.4, entry 7), the formula is $u = 20k - 5k = 15k$, $k = 5$, the last hyper-ring unit being omitted because of the cyclic structure. Thus, the drop in g is of 5 units for each fivefold hyper-cycle (compare Table 8.4, entries 6 and 7).

In case of the spherical array BMTZSp20_12 (Table 8.4, entry 9), $u = 20k - 2[5(k-1)]$, $k = 12$. Remark the twice subtraction of the term $5(k-1)$, in case of the spherical array, which accounts for the difference in g to the linear array of $k = 12$ (Table 8.4, entries 8 and 9): $186 - 131 = 55 = 5(12-1)$. This drop in g, in case of the spherical array, seems to parallel the well-known result that sphere is the minimal surface among all known solid objects. The number u is also related to the number of simple faces/rings as follows: $u = f_8/6$ in case BMTA and $u = f_6/4$ in case BMTZ.

On the ground of Theorem 8.1, the spherical array BMTZSp20_12 seems to be the *minimum* g (lower bound) while BMTZ20_k the *maximum* g (upper bound) among all the studied structures (Diudea and Szefler 2012). We just demonstrated the following:

Theorem 8.2 *The genus in multi-tori shows the lower-bound value in structures of icosahedral symmetry, while the upper-bound value is shown in linear structures provided the same number of* (*open*) *tetrahedral units.*

Note these icosahedral multi-tori represent quasicrystal nanostructures; quasicrystals have been Nobel prized in 2011.

Carbon atom *orbit analysis* in BMTZSp20_12 revealed a 6.8^2 massive class (2,580 atoms, about 83 %), located inside, of the same signature as in polybenzene, and two smaller classes, of signature 6.8 (360 atoms), and 6 (180 atoms), disposed outside of the spherical structure. Compare with % of 6.8^2 in the linear array BMTZ20_k (about 74 % at $k = 12$) and in BMTA20_k (about 26 %, at $k = 9$). Knowing the (calculated by O'Keeffe et al. 1992) stability of polybenzene, consisting of only 6.8^2 atoms (in the infinite triple periodic net), the orbit analysis provides a "topological" proof of stability of the spherical array BMTZSp20_12 (Diudea and Szefler 2012).

8.6 Omega Polynomial in Polybenzenes

In a connected graph $G(V, E)$, with the vertex set $V(G)$ and edge set $E(G)$, two edges $e = uv$ and $f = xy$ of G are called *codistant e co f* if they obey the relation (John et al. 2007)

$$d(v, x) = d(v, y) + 1 = d(u, x) + 1 = d(u, y) \tag{8.7}$$

which is reflexive, that is, *e co e* holds for any edge e of G, and symmetric, if *e co f*, then *f co e*. In general, relation *co* is not transitive; if "*co*" is also transitive, thus it is an equivalence relation, then G is called a *co-graph*, and the set of edges $C(e) := \{f \in E(G); f \ co \ e\}$ is called an *orthogonal cut oc* of G, $E(G)$ being the union of disjoint orthogonal cuts: $E(G) = C_1 \cup C_2 \cup \ldots \cup C_k$, $C_i \cap C_j = \emptyset, i \neq j$. Klavžar (2008) has shown that relation *co* is a theta Djoković (1973)–Winkler (1984) relation.

We say that edges e and f of a plane graph G are in relation *opposite*, *e op f*, if they are opposite edges of an inner face of G. Note that the relation *co* is defined in the whole graph while *op* is defined only in faces. Using the relation *op*, we can partition the edge set of G into *opposite* edge *strips*, *ops*. An *ops* is a quasi-orthogonal cut *qoc*, since *ops* is not transitive.

Let G be a connected graph and $S_1, S_2, \ldots, S_k$ be the *ops* strips of G. Then, the *ops* strips form a partition of $E(G)$. The length of *ops* is taken as maximum. It depends on the size of the maximum-fold face/ring $F_{\max}/R_{\max}$ considered so that any result on Omega polynomial will have this specification.

Denote by $m(G,s)$ the number of *ops* of length s and define the Omega polynomial as (Diudea 2006; Diudea et al. 2006b, 2008, 2009; Ashrafi et al. 2008; Diudea and Klavžar 2010; Vizitiu et al. 2007)

$$\Omega(G, x) = \sum_s m(G, s) \cdot x^s \tag{8.8}$$

Its first derivative (in $x = 1$) equals the number of edges in the graph:

$$\Omega'(G, 1) = \sum_s m(G, s) \cdot s = e = |E(G)| \tag{8.9}$$

On Omega polynomial, the Cluj-Ilmenau index (John et al. 2007), $\mathrm{CI} = \mathrm{CI}(G)$ was defined:

$$\mathrm{CI}(G) = \{[\Omega'(G, 1)]^2 - [\Omega'(G, 1) + \Omega''(G, 1)]\} \tag{8.10}$$

Formulas to calculate Omega polynomial and CI index in three infinite networks, f_{cc}-BTA_48 (Fig. 8.11), *p*-BCZ_48 (Fig. 8.10, top), and *p*-BCA_96 (Fig. 8.10, bottom), are listed in Table 8.5. Formulas were derived from the numerical data

Table 8.5 Omega polynomial and net parameters in polybenzene networks

Net	Omega polynomial
BTA_48	$R_{\max}(8)$
	$\Omega(\text{BTA\_48}) = 18k^2X^2 + 6k(k-1)X^{2k} + 6kX^{4k} + \sum_{s=1}^{k-1} 12kX^{4s}$
	$\Omega'(1) = 12k^2(3k+2) = \lvert E(G)\rvert$ = edges
	$\text{CI}(G) = 8k^2(162k^4 + 216k^3 + 61k^2 + 3k - 13)$
	atoms $= 24k^2(k+1) = \lvert V(G)$
	$R_6 = 4k^3$; $R_8 = 6k^3 - 3k^2 + 3k$
	$R_{\max}(12)$
	$\Omega(\text{BTA\_48}) = 6X^{2k(2k+1)} + 3X^{4k^2(k+1)} + \sum_{s=1}^{k-1} 12X^{2s(2k+1)}$
	$\Omega'(1) = 12k^2(3k+2) = \lvert E(G)\rvert$ = edges
	$\text{CI}(G) = 8k(6k^2 + 2k - 1)(26k^3 + 24k^2 + 6k + 1)$
	$R_{12} = 4k^3$
Examples	$R_{\max}(8)$
	$k = 5$; $\Omega(G) = 450X^2 + 60X^4 + 60X^8 + 120X^{10} + 60X^{12} + 60X^{16} + 30X^{20}$;
	CI = 25,955,400; atoms = 3,600; edges = 5,100; $R_6 = 500$; $R_8 = 690$
	$k = 6$; $\Omega(G) = 648X^2 + 72X^4 + 72X^8 + 252X^{12} + 72X^{16} + 72X^{20} + 36X^{24}$;
	CI = 74,536,992; atoms = 6,048; edges = 8,640; $R_6 = 864$; $R_8 = 1{,}206$
	$R_{\max}(12)$
	$k = 5$; $12X^{22} + 12X^{44} + 12X^{66} + 12X^{88} + 6X^{110} + 3X^{600}$;
	CI = 246,831,60; $R_{12} = 500$
	$k = 6$; $12X^{26} + 12X^{52} + 12X^{78} + 12X^{104} + 12X^{130} + 6X^{156} + 3X^{1008}$;
	CI = 71,009,232; $R_{12} = 864$
BCZ_48	$R_{\max}(8)$
	$\Omega(\text{BCZ\_48}) = 12kX + 12k(k+1)X^2 + 3k(k-1)(2k-1)X^4 + \sum_{s=1}^{k-1} 24kX^{(2+4s)}$
	$\Omega'(1) = 12k^2(6k-1) = \lvert E(G)\rvert$ = edges
	$\text{CI}(G) = 4k(1,296k^5 - 432k^4 + 4k^3 - 24k^2 + 32k - 3)$
	atoms $= 48k^3 = \lvert V(G)\rvert$
	$R_6 = (2k)^3$; $R_8 = 12k^2(k-1)$
	$R_{\max}(12)$
	$\Omega(\text{BCZ\_48}) = (6k-3)X^{(2k)^2} + 6X^{(2k)^3}$
	$\Omega'(1) = 12k^2(6k-1) = \lvert E(G)\rvert$ = edges
	$\text{CI}(G) = 96k^4\left(50k^2 - 19k + 2\right)$
	$R_{12} = 6k\left(2k^2 - 2k + 1\right)$
Examples	$R_{\max}(8)$
	$k = 5$; $60X + 360X^2 + 540X^4 + 120X^6 + 120X^{10} + 120X^{14} + 120X^{18}$
	CI = 75,601,140; atoms = 6,000; edges = 8,700; $R_6 = 1{,}000$; $R_8 = 1{,}200$.
	$k = 6$; $72X + 504X^2 + 990X^4 + 144X^6 + 144X^{10} + 144X^{14} + 144X^{18} + 144X^{22}$
	CI = 228,432,312; atoms = 10,368; edges = 15,120; $R_6 = 1{,}728$; $R_8 = 2{,}160$.
	$R_{\max}(12)$
	$k = 5$; $27X^{100} + 6X^{1000}$; CI = 69,420,000; $R_{12} = 1{,}230$.
	$k = 6$; $33X^{144} + 6X^{1728}$; CI = 210,014,208; $R_{12} = 2{,}196$.

(continued)

Table 8.5 (continued)

Net	Omega polynomial
BCA_96	$R_{\max}(8)$ $\Omega(\text{BCA\_96}) = 36kX^2 + 12k(k-1)X^3 + 3(k-1)(k^2-k+8)X^4$ $+24(k-1)X^8 + 12k^2X^{4k} + \sum_{s=0}^{k-3} 24(k-s-2)(X^{10+6s} + X^{14+6s})$ $\Omega'(1) = 12k^2(9k+1) = \lvert E(G)\rvert$ = edges $\text{CI}(G) = 12k(972k^5 + 216k^4 - 16k^3 - 4k^2 + 3k + 1)$ atoms $= 24k^2(3k+1) = \lvert V(G)\rvert$ $R_6 = 4k(5k-3)$; $R_8 = 12k^3$; $R_{12} = 6k(k-1)^2$
Examples	$R_{\max}(8)$ $k=5$; $\Omega(G) = 180X^2 + 240X^3 + 336X^4 + 96X^8 + 72X^{10} + 72X^{14} + 48X^{16}$ $+ 348X^{20} + 24X^{22} + 24X^{26}$ CI = 190,224,960; atoms = 9,600; edges = 13,800; $R_6 = 2{,}200$; $R_8 = 1{,}500$. $k=6$; $\Omega(G) = 216X^2 + 360X^3 + 570X^4 + 120X^8 + 96X^{10} + 96X^{14} + 72X^{16}$ $+ 72X^{20} + 48X^{22} + 432X^{24} + 48X^{26} + 24X^{28} + 24X^{32}$ CI = 564,093,144; atoms = 16,416; edges = 23,760; $R_6 = 3{,}888$; $R_8 = 2{,}592$

calculated on cuboids of (k, k, k) dimensions by the Nano Studio software (Nagy and Diudea 2009). Omega polynomial was calculated at $R_{\max}(8)$ and $R_{\max}(12)$, respectively; examples are given in view of an easy verification of the general formulas. Also, formulas for the number of atoms, edges, and rings (R_6, R_8 and R_{12}) are included in this table (Szefler and Diudea 2012).

Formulas to calculate Omega polynomial and CI index in the two infinite networks BMTA20k and BMTZ20k, designed on the ground of BMTA1_48 and BMTZ1_24 units, are presented in Tables 8.6 and 8.7. Formulas were derived from the numerical data calculated on rods consisting of k units BMTX20. Omega polynomial was calculated at $R_{\max} = R_8$. Formulas for the number of atoms, edges, and rings (R_6, R_8, and R_{15}, the last one being the simple ring of the hyper-ring BMTACy5) are included in Tables 8.6 and 8.7. Numerical examples are also given (Diudea and Szefler 2012).

Omega polynomial description can be looked as an alternative to the crystallographic description, helping in understanding the topology of these networks.

8.7 Conclusions

Spanning fullerenes can be obtained by deleting some atoms or bonds from the graph of closed fullerenes, thus resulting in open structures which can further join to atoms of the same or different repeating units in construction of crystal- or quasicrystal-like networks. A variety of spanning fullerenes, designed either by cage opening or by sequences of map operations, has been used to build nano-dendrimers

Table 8.6 Formulas for Omega polynomial and net parameters in linear periodic BMTA20_k network

BMTA20_k	$R_{\max}(8)$;
	$\Omega(\text{BMTA20}\_k\_R_8) = 10(k+2)X^3+5(k-1)X^4+(11k+1)X^5+20(k+3)X^8$
	$+10(k-1)X^{10}+15(k-1)X^{12}+(11k+1)X^{20}+10X^{2(3k+1)}$
	$\Omega'(1) = 825k + 285 = \lvert E(G)\rvert$ = edges;
	$\text{CI}(G) = 15\left(45,351k^2 + 30,715k + 5,332\right)$;
	atoms $= 10(57k + 21) = \lvert V(G)\rvert$;
	$R_6 = 5(27k + 7)$; $\quad R_8 = 30(3k + 1)$; $R_{15} = 11k + 1$
	$u_{48} = 20k - 5(k - 1) = 5(3k + 1) = R_8/6$;
	$g = 1 + u_{48}$
Examples	$k = 5$;
	CI = 19,390,230; atoms = 3,060; edges = 4,410; $R_6 = 710$; $R_8 = 480$; $R_{15} = 56$;
	$u_{48} = 80$; $g = 81$.
	$k = 6$;
	CI = 27,333,870; atoms = 3,630; edges = 5,235; $R_6 = 845$; $R_8 = 570$; $R_{15} = 67$;
	$u_{48} = 95$; $g = 96$.

Table 8.7 Formulas for Omega polynomial and net parameters in linear periodic BMTZ20_k network

BMTZ20_k	$R_{\max}(8)$
	$\Omega(\text{BMTZ20}\_k\_R_8) = 10(k+2)X^2 + 30kX^3 + (11k+1)X^5 + 10(k+5)X^6$
	$+ 10(k-1)X^8 + 10(k-1)X^{10} + 6kX^{20}$
	$\Omega'(1) = 525k + 165 = \lvert E(G)\rvert$ = edges
	$\text{CI}(G) = 5\left(55,125k^2 + 33,653k + 5,392\right)$
	atoms $= 120(3k + 1) = \lvert V(G)\rvert = 24u_{24} = 6R_6$
	$R_6 = 20(3k + 1) = \lvert V(G)\rvert/6$; $\quad R_8 = 15(5k + 1)$; $\quad R_{15} = 11k + 1$
	$u_{24} = 20k - 5(k - 1) = 5(3k + 1) = R_6/4$;
	$g = 1 + u_{24}$
Examples	$k = 5$; $70X^2 + 150X^3 + 56X^5 + 100X^6 + 40X^8 + 40X^{10} + 30X^{20}$
	CI = 7,758,910; atoms = 1,920; edges = 2,790; $R_6 = 320$; $R_8 = 390$; $R_{15} = 56$;
	$u_{24} = 80$; $g = 81$
	$k = 6$; $80X^2 + 180X^3 + 67X^5 + 110X^6 + 50X^8 + 50X^{10} + 36X^{20}$
	CI = 10,959,050; atoms = 2,280; edges = 3,315; $R_6 = 380$; $R_8 = 465$; $R_{15} = 67$;
	$u_{24} = 95$; $g = 96$

and crystal- and quasicrystal-like structures. Energetics of some open fullerenes has been calculated on optimized structures at Hartree-Fock and/or DFT level of theory. All of the discussed open fullerenes have shown less strained structures in comparison to C_{60} reference fullerene, while the overall stability, as suggested by the total energy and HOMO-LUMO gap, is comparable or even better to the reference fullerene, thus being candidates to the status of real molecules. Omega polynomial was used to describe the topology of some periodic networks, designed by using benzene as the simplest patch.

Acknowledgments The work was supported in part by the Romanian CNCSIS-UEFISCSU project PN-II-ID-PCE-2011-3-0346 and in part by the computational grant no. 133 of PCSS (Poznań, Poland).

References

Ashrafi AR, Jalali M, Ghorbani M, Diudea MV (2008) MATCH Commun Math Comput Chem 60:905
Benedek G, Vahedi-Tafreshi H, Barborini E, Piseri P, Milani P, Ducati C, Robertson J (2003) Diamond Relat Mater 12:768
Blase X, Benedek G, Bernasconi M (2010) In: Colombo L, Fasolino A (eds) Computer-based modeling of novel carbon systems and their properties. Beyond nanotubes. Springer, Dordrecht, p 171
Bonnet O (1853) CR Acad Sci Paris 37:529
Cysewski P, Szefler B (2010) J Mol Model 16:1709
Diudea MV (2004) Forma (Tokyo) 19:131
Diudea MV (2005) J Chem Inf Model 45:1002
Diudea MV (2006) Carpath J Math 22:43
Diudea MV (2010a) Nanomolecules and nanostructures – polynomials and indices, vol 10. University of Kragujevac, Serbia
Diudea MV (2010b) Int J Chem Model 2:155
Diudea MV (2010c) MATCH Commun Math Comput Chem 63:247
Diudea MV (2010d) Studia Univ Babes Bolyai Chemia 55(4):11
Diudea MV, Katona G (1999) In: Newkome GA (ed) Advances in dendritic macromolecules. JAI Press Inc. Stamford, Connecticut, vol 4, p 135
Diudea MV, Klavžar S (2010) Acta Chim Slov 57:565
Diudea MV, Nagy CL (2007) Periodic nanostructures. Springer, Dordrecht
Diudea MV, Petitjean M (2008) Symmetry Cult Sci 19(4):285
Diudea MV, Gutman I, Jäntschi L (2002) Molecular topology. NOVA, New York
Diudea MV, John PE, Graovac A, Primorac M, Pisanski T (2003) Croat Chem Acta 76:153
Diudea MV, Cigher S, Vizitiu AE, Ursu O, John PE (2006a) Croat Chem Acta 79:445
Diudea MV, Stefu M, John PE, Graovac A (2006b) Croat Chem Acta 79:355
Diudea MV, Cigher S, John PE (2008) MATCH Commun Math Comput Chem 60:237
Diudea MV, Cigher S, Vizitiu AE, Florescu MS, John PE (2009) J Math Chem 45:316
Diudea MV, CsL N, Ilić A (2011) In: Putz MV (ed) Carbon bonding and structures. Springer, Dordrecht/Heidelberg/London/New York, p 273
Diudea MV, Szefler B (2012) Nanotube junctions and the genus of multi-tori. Phys Chem Chem Phys 14:8111–8115
Djoković DŽ (1973) J Comb Theor Ser B 14:263
Euler L (1758) Novi Commun Acad Sci Imp Petrop 4:109
Gaussian 09, (2009) Revision A.1, Frisch MJ, Trucks GW, Schlegel HB, Scuseria GE, Robb MA, Cheeseman JR, Scalmani G, Barone V, Mennucci B, Petersson GA, Nakatsuji H, Caricato M, Li X, Hratchian HP, Izmaylov AF, Bloino J, Zheng G, Sonnenberg JL, Hada M, Ehara M, Toyota K, Fukuda R, Hasegawa J, Ishida M, Nakajima T, Honda Y, Kitao O, Nakai H, Vreven T, Montgomery JA, Peralta JE, Ogliaro F, Bearpark M, Heyd JJ, Brothers E, Kudin KN, Staroverov VN, Kobayashi R, Normand J, Raghavachari K, Rendell A, Burant JC, Iyengar SS, Tomasi J, Cossi M, Rega N, Millam NJ, Klene M, Knox JE, Cross JB, Bakken V, Adamo C, Jaramillo J, Gomperts R, Stratmann RE, Yazyev O, Austin AJ, Cammi R, Pomelli C,

Ochterski JW, Martin RL, Morokuma K, Zakrzewski VG, Voth GA, Salvador P, Dannenberg JJ, Dapprich S, Daniels AD, Farkas Ö, Foresman JB, Ortiz JV, Cioslowski J, Fox DJ, Gaussian Inc, Wallingford
Haddon RC (1987) J Am Chem Soc 109:1676
Haddon RC (1990) J Am Chem Soc 112:3385
Harary F (1969) Graph theory. Addison – Wesley, Reading
Hargittai M, Hargittai I (2010) Symmetry through the eyes of a chemist. Springer, Dordrecht/London/New York/Heidelberg, p 488
John PE, Vizitiu AE, Cigher S, Diudea MV (2007) MATCH Commun Math Comput Chem 57:479
Klavžar S (2008) MATCH Commun Math Comput Chem 59:217
Krygowski TM, Ciesielski A (1995) J Chem Inf Comput Sci 35:203
Krygowski TM, Cyranski M (1996) Tetrahedron 52:1025564
Lenosky T, Gonze X, Teter M, Elser V (1992) Nature 355:333
Levine D, Steinhardt PJ (1984) Phys Rev Lett 53:2477
Mackay AL (1981) Kristallografiya (Sov Phys Chrystallogr) 26:910 (517)
Mackay AL, Terrones H (1991) Nature 352:762
Nagy CL, Diudea MV (2009) Nano studio software. Babes-Bolyai University, Cluj
Nagy K, Nagy CL, Diudea MV (2011) MATCH Commun Math Comput Chem 65:163
O'Keeffe M, Adams GB, Sankey OF (1992) Phys Rev Lett 68:2325
Schwarz HA (1865) Über Minimalflächen, Monatsber. Berlin Akad
Schwarz HA (1890) Gesammelte Matematische Abhandlungen. Springer, Berlin
Stefu M, Diudea MV (2005) CVNET software. Babes-Bolyai University, Cluj
Stefu M, Diudea MV, John PE (2005) Studia Univ Babes Bolyai Chemia 50(2):165
Szefler B, Diudea MV (2012) Polybenzene revisited. Acta Chim Slov 59:795–802
Szefler B, Saheli M, Diudea MV (2012a) Sumanene units in P-type surface networks. Acta Chim Slov 59:177–182
Szefler B, Ponta O, Diudea MV (2012b) Energetics of polybenzene multi tori. J Molec Struct 1022:89–93
Szefler B, Diudea MV (2013) Strain in Platonic fullerenes. Struct Chem. doi:10.1007/s11224-013-0244-y
Terrones H, Mackay AL (1993) Chem Phys Lett 207:45
Vizitiu AE, Cigher S, Diudea MV, Florescu MS (2007) MATCH Commun Math Comput Chem 57:457
Winkler PM (1984) Discrete Appl Math 8:209